Supplemental Figure S1

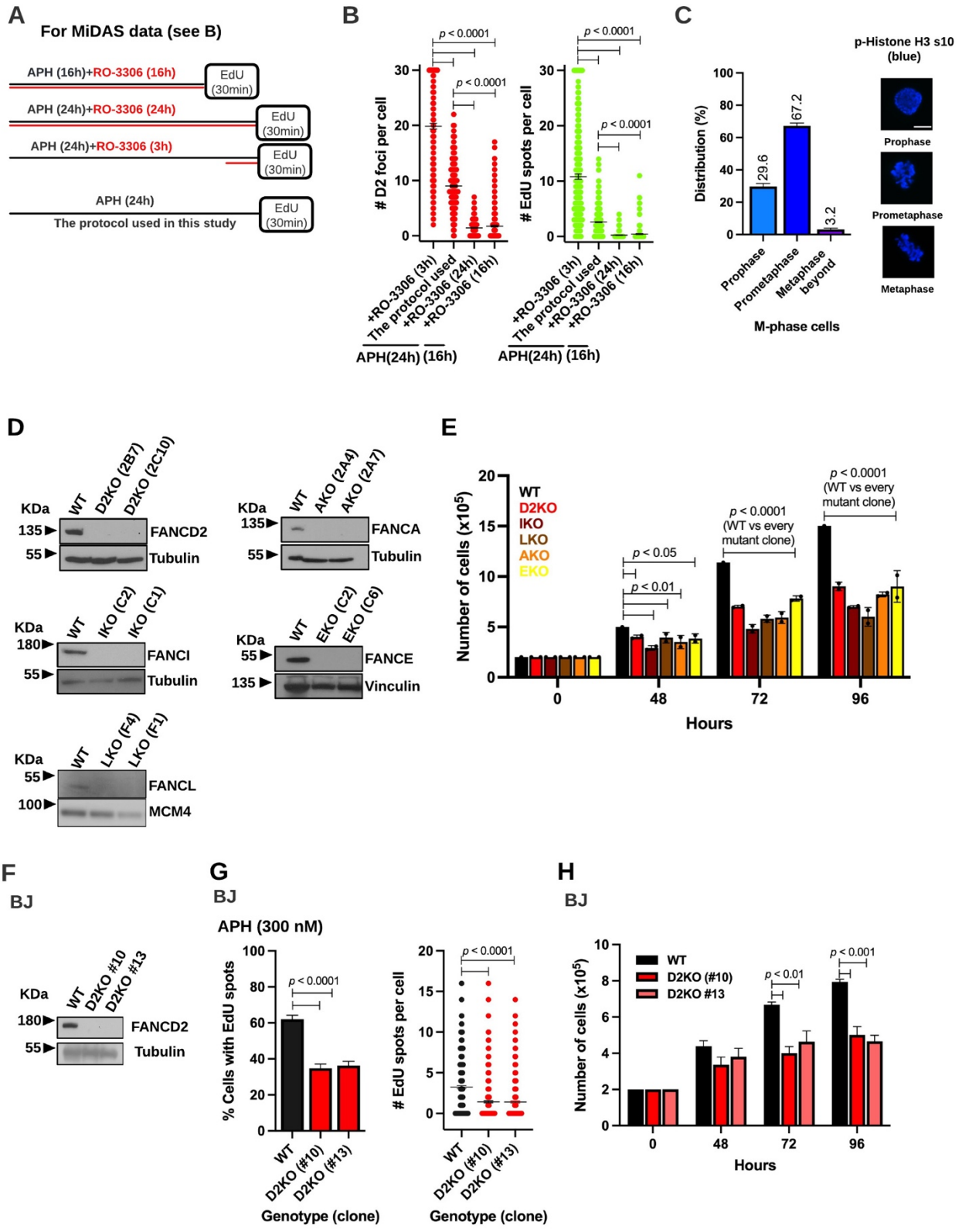

Supplemental Figure S1. Validation of the experimental design for MiDAS used in this study as well as confirmation of RPE1 FA mutant clones and phenotypes of BJ *FANCD2* KO clones.
A) Several experimental schemes for the induction of MiDAS were tested for suitability in RPE1 cells during which EdU pulse labeling occurred for 30 min. Simultaneous treatment with 300 nM APH and 10 μM RO-3306 (CDK1 inhibitor) for either 16 or 24 hrs resulted in lower MiDAS levels than those observed after APH-treatment alone (see **B**). We suspected that a long G2 arrest by the CDK1 inhibitor promotes the resolution of late replication intermediates as reported for chromosome lesions (Boteva et al. 2020). Therefore, we limited the introduction of RO-3306 to the last 3 hrs of the 24 hr-APH treatment. Under this condition, we saw a substantial increase in FANCD2 foci and EdU spots, indicating the exacerbation of replication stress by RO-3306. Given the reported off-target effect (Mocanu et al. 2022), these unexpected outcomes of RO-3306 use led us to conclude that the experimental schemes involving the CDK1 inhibitor are not suitable to analyze MiDAS in this cell line. According to a preceding study (Minocherhomji et al. 2015), a 30 min incubation with EdU upon release from RO-3306 treatment captures EdU uptake up until prometaphase. In keeping with these findings, we also observed very few M-phase cells that reached metaphase or beyond under similar conditions (see **C**). Therefore, we used a 30 min pulse length without RO-3306 treatment in this study.
B) Numbers of FANCD2 (D2) foci (left) and EdU spots (right) per early M-phase cell for the experimental conditions described in **A**. Midlines indicate means, and bars show standard errors. Experiments were repeated three times. For each condition, at least 300 cells were scored. Pooled data (shown here) were analyzed for significances using a Mann-Whitney test.
C) The distribution of M-phase cells (prophase, prometaphase, and metaphase/beyond indicated by respective microscope photos) observed within 30 mins upon release from simultaneous 16-hr APH and RO-3306 treatment. A total of 598 RPE1 cells positive for phospho-Histone H3 were scored in three trials. Bars indicate standard errors. The scale bar indicates 10 μm.
D) Immunoblotting of whole cell lysate (WCL) confirms the lack of FANCD2 (top left), FANCI (middle left), FANCL (bottom left), FANCA (top right), and FANCE (bottom right) KO clones as well as the levels of relevant proteins in their parental WT RPE1 cells. Vinculin, Tubulin, and MCM4 were used as loading controls.
E) Cell proliferation data for RPE1 WT cells and the FA mutants. Cells were seeded in triplicate using 6-well plates at a density of $2x10^5$ cells per well. At 48, 72, and 96-hr time points, cells were trypsinized and numbers of live cells were counted by the Countess II Automated Cell Counter (Thermo Fisher Scientific) using a trypan blue exclusion method. Experiments were repeated three times, and pooled data are shown here. The column for each genotype indicates the average of two clones, with each clone indicated by dots. Significances were calculated using a t-test.
F) Immunoblotting of WCL confirming the lack of FANCD2 in BJ D2KO clones #10 and #13 with WT BJ cells used as a control. Tubulin was used as a loading control.
G) Percentages of early M-phase cells positive for EdU (left) and numbers of EdU spots per cell (right) for each BJ D2KO clone and WT cells. Midlines in the right-side panel show means, and bars indicate standard errors. Experiments were repeated at least three times, and a minimum of 400 nuclei were scored per genotype/clone. Pooled data (shown here) were analyzed for significances using a χ^2 test (left) or a Mann-Whitney test (right).
H) Cell proliferation data for BJ D2KO clones and WT cells. The average number of live cells at 48-, 72-, and 96-hr time points are shown for each D2KO mutant clone and WT. Experiments were repeated three times, and pooled data are shown here. After 72 hrs, both D2KO clones

show a significant growth defect as seen in RPE1 D2KO clones. Bars indicate standard errors. Significances were calculated using a t-test.

Supplemental Figure S2

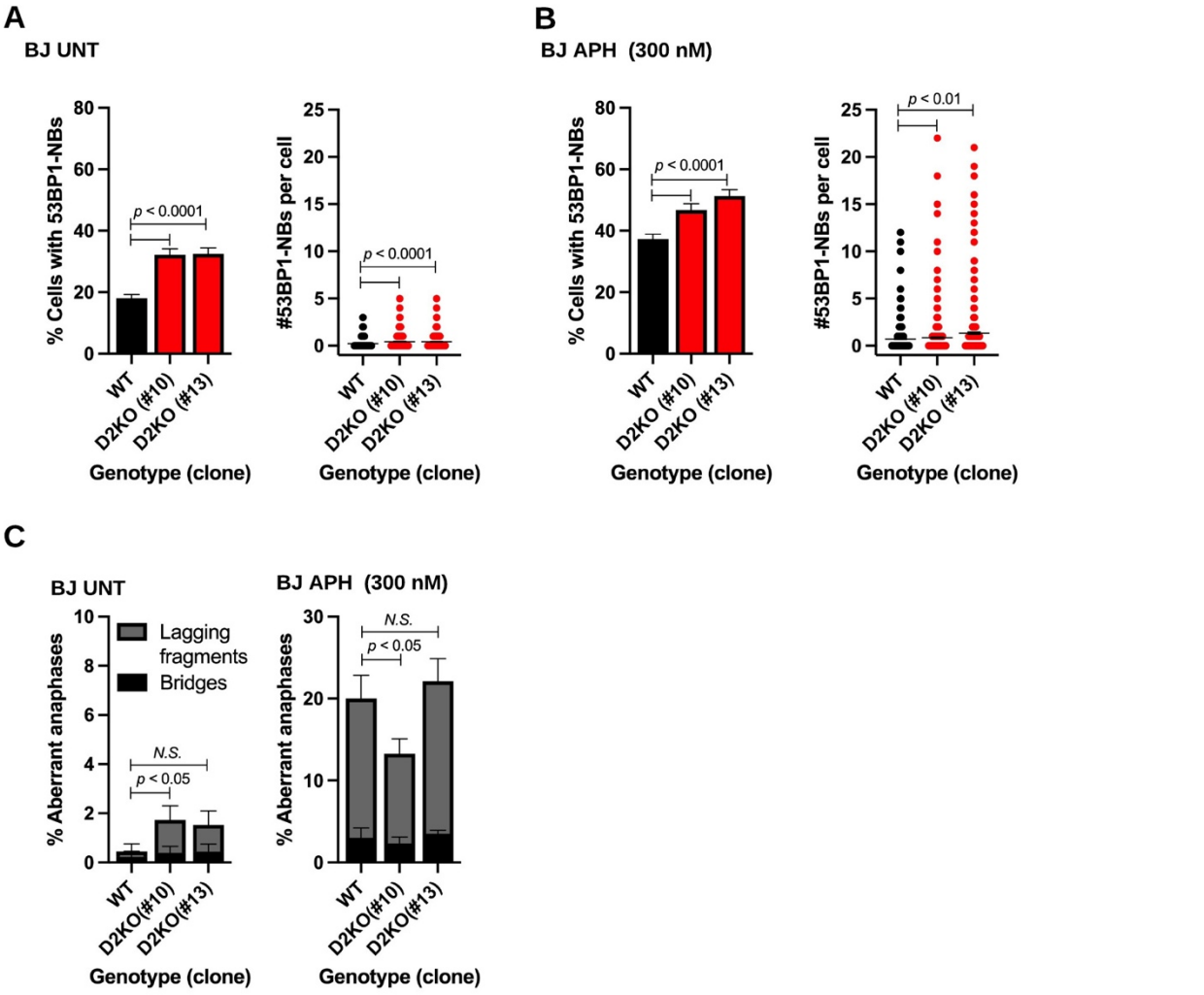

Supplemental Figure S2. FANCD2 deficiency in BJ cells moderately elevates 53BP1-NBs but not aberrant anaphases upon APH treatment.
A) Percentages of G1-phase cells with 53BP1-NBs (left) and numbers of 53BP1-NBs per cell with means indicated by midlines (right) in untreated BJ D2KO clones as well as WT cells.
B) Percentages of G1-phase cells with 53BP1-NBs (left) and numbers of 53BP1-NBs per cell with means indicated by midlines (right) in APH-treated BJ D2KO clones as well as WT cells.
C) Percentages of aberrant anaphases observed in the D2KO clones and WT cells in untreated (left) and APH-treated (right) conditions. The proportion of anaphases with either lagging chromosomes or bridges are shown in gray and black, respectively.
In **A-C**, bars indicate standard errors. Experiments were repeated at least three times, and a minimum of 600 nuclei/400 anaphases were scored per genotype/clone. Pooled data (shown here) were analyzed for significances using a χ^2 test (**A-B** left, and **C**) or a Mann-Whitney test (**A-B** right).

Supplemental Figure S3

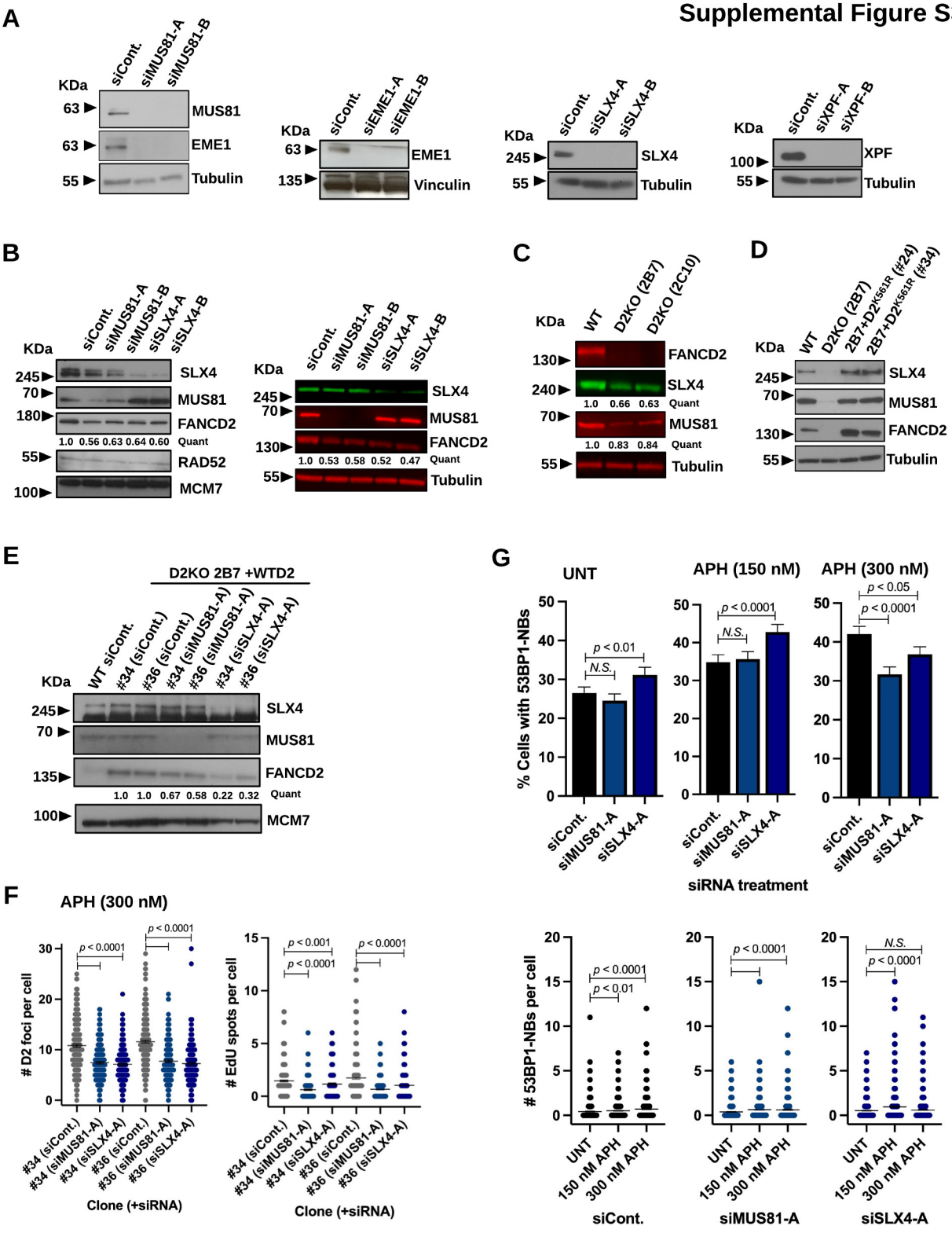

Supplemental Figure S3. Depletion of MUS81, EME1, or SLX4 decreases FANCD2 protein levels but has little effect on the induction of 53BP1-NBs in RPE1 cells.
A) Immunoblotting of WCL confirming depletion of MUS81, EME1, SLX4, or XPF respectively via two independent siRNAs using siControl-treated WT used as a control. Note that MUS81 depletion also lowers EME1 levels. Vinculin and Tubulin were used as loading controls.
B) Immunoblotting of two independently prepared sets of WCL showing reproducibly decreased levels of FANCD2 after depletion of MUS81 or SLX4 regardless of enhanced chemiluminescence (ECL, left) or fluorescent (right) based detection. MUS81 depletion resulted in decreased levels of SLX4, whereas SLX4 depletion had little effect on MUS81 levels. RAD52 showed little change in its levels after depletion of MUS81 or SLX4 (left).
C) Fluorescent immunoblotting showing that the D2KO clones 2B7 and 2C10 exhibit reciprocally decreased levels of MUS81 and SLX4 compared to WT cells.
D) Immunoblotting of WCL detected by ECL reproducibly showing increased levels of MUS81 and SLX4 in the D2KO 2B7 over-expressing $D2^{K561R}$ clones #24 and #34 relative to the parental 2B7 clone in conjunction with **Fig. 4E**. Tubulin was used as a loading control.
E) Immunoblotting of WCL shows decreased levels of FANCD2 in the D2KO 2B7 over-expressing WTD2 clones #34 and #36 upon MUS81 or SLX4 depletion compared to siControl treated conditions. WT cells treated with siControl were used as a reference for the endogenous FANCD2 level. MCM7 was used as a loading control.
F) Numbers of FANCD2 foci (left) and those of EdU spots (right) per cell for the D2KO 2B7 over-expressing WTD2 clones #34 and #36 after treatment with siControl, siMUS81, or siSLX4 in APH-treated conditions. Midlines indicate means, and bars indicate standard errors. Experiments were repeated at least three times, and a minimum of 200 nuclei were scored per treatment. Pooled data (shown here) were analyzed for significances using a Mann-Whitney test.
G) Percentages of G1-phase cells with 53BP1-NBs after depletion of MUS81 or SLX4 in comparison to siControl-treated cells in untreated (top left), 150 nM APH-(top middle), and 300 nM APH (top right)-treated conditions as well as numbers of 53BP1-NBs per cell for siControl-(bottom left), siMUS81- (bottom middle), and siSLX4- (bottom right) treated conditions. A significant, APH dose-dependent increase in 53BP1-NBs was observed in cells treated with siControl but not in MUS81- or SLX4-treated cells. Midlines indicate means in the bottom panels, and bars indicate standard errors. Experiments were repeated at least three times, and a minimum of 600 nuclei were scored per treatment. Pooled data (shown here) were analyzed for significances using a χ^2 test (top) or a Mann-Whitney test (bottom).
In **B, C,** and **E** quantifications shown for the representative blots were normalized to the loading control and calculated relative to the relevant siControl using ImageJ for ECL-based imaging and Image Studio for fluorescence-based imaging. MCM7 and Tubulin were used as loading controls.

Supplemental Figure S4

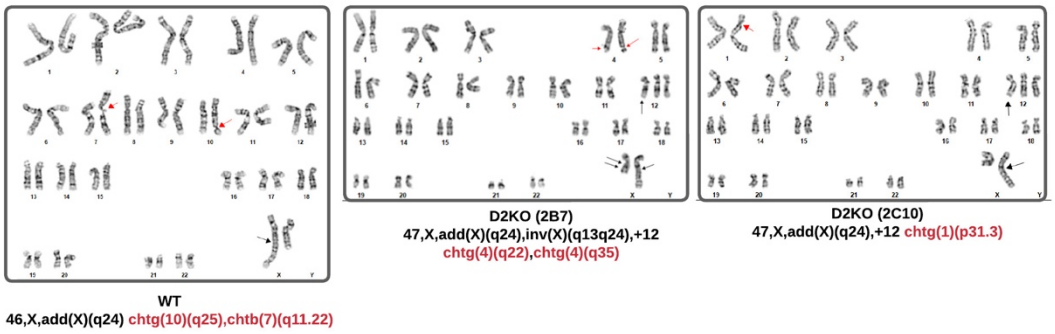

Supplemental Figure S4. G-banded karyotype images from RPE1 WT cells as well as the D2KO 2B7 and 2C10 clones. Preexisting abnormal chromosomes or aneuploidy are marked with black arrows. APH-induced chromosomal aberrations are marked with red arrows, and are categorized as chromatid gaps (chtg), chromatid breaks (chtb), or chromosome breaks (chrb). The location of each abnormality is described below the relevant karyotype.

Supplemental Figure S5

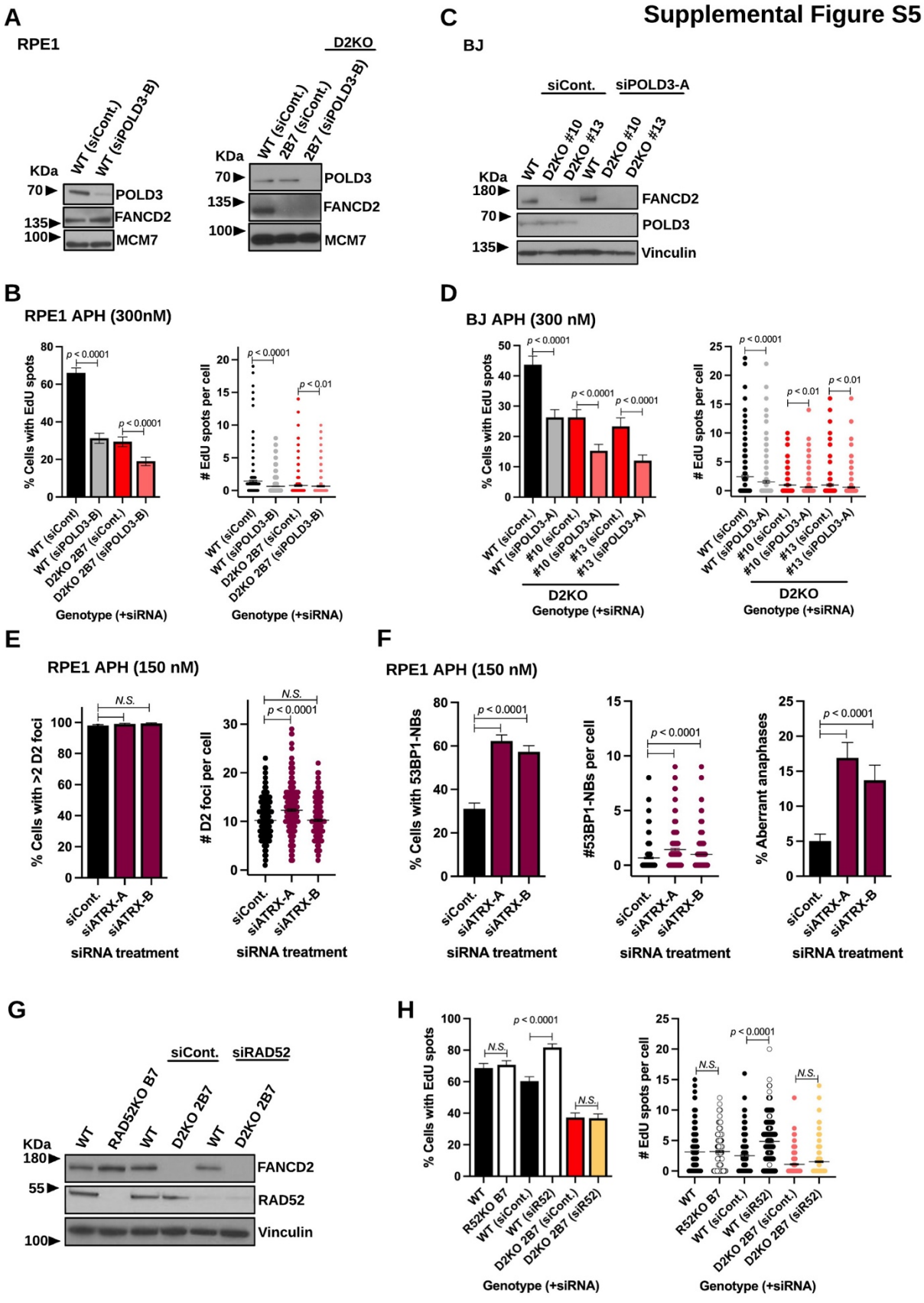

Supplemental Figure S5. Residual MiDAS in RPE1 and BJ D2KO clones depends on POLD3 and ATRX depletion increases 53BP1-NBs and aberrant anaphases in RPE1 cells.
A) Immunoblotting of WCL confirming depletion of POLD3 via a second siPOLD3 (siPOLD3-B) in comparison to siControl treated conditions in RPE1 WT cells (left) and the D2KO 2B7 clone (right). MCM7 was used as a loading control.
B) Percentages of early M-phase cells positive for EdU spots (left) and numbers of EdU spots per cell (right) in RPE1 WT cells and the 2B7 clone treated with siPOLD3-B or siControl. Midlines on the right-side panel indicate means, and bars indicate standard errors. Experiments were repeated at least three times, and a minimum of 300 nuclei were scored per treatment. Pooled data (shown here) were analyzed for significances using a χ^2 test (left) or a Mann-Whitney test (right).
C) Immunoblotting of WCL confirming depletion of POLD3 in comparison to siControl treated conditions in BJ WT and the D2KO clones. Vinculin was used as a loading control.
D) Percentages of early M-phase cells positive for EdU spots (left) and numbers of EdU spots per cell (right) in BJ WT cells and the D2KO clones treated with siPOLD3-A or siControl. Midlines on the right-side panel indicate means, and bars indicate standard errors. Experiments were repeated at least three times, and a minimum of 200 nuclei were scored per treatment. Pooled data (shown here) were analyzed for significances using a χ^2 test (left) or a Mann-Whitney test (right).
E) Percentages of early M-phase cells with >2 FANCD2 (D2) foci (left) and number of D2 foci per cell with means shown as midlines (right) after respective siRNA treatments in conjunction with **Fig. 6F**. Significances were calculated using a χ^2 test (left) or a Mann-Whitney test (right).
F) Percentages of G1-phase RPE1 cells with 53BP1-NBs (left), numbers of 53BP1-NBs per cell with means shown as midlines (middle), and percentages of aberrant anaphases (right) after depletion of ATRX in comparison to siControl-treated cells. Significances were calculated using a χ^2 test (left, right) or a Mann-Whitney test (middle).
In **E** and **F,** bars indicate standard errors. Experiments were repeated at least three times, and a minimum of 300 nuclei/anaphases were scored per treatment. Pooled data are shown.
G) Immunoblotting of WCL confirming the absence of RAD52 in RAD52KO clone B7 and depletion of RAD52 in WT and the D2KO 2B7 clone. Vinculin was used as a loading control.
H) Percentages of early M-phase cells positive for EdU spots (left) and numbers of EdU spots per cell (right) for WT cells and RAD52KO clone B7, as well as WT cells and the D2KO clone 2B7 after treatment with siControl and siRAD52 (siR52) in APH-treated conditions. Bars indicate standard errors. Experiments were repeated at least three times, and a minimum of 300 nuclei/anaphases were scored per treatment. Pooled data (shown here) were analyzed for significances using a χ^2 test (left) or a Mann-Whitney test (right).

Supplementary Figure S6

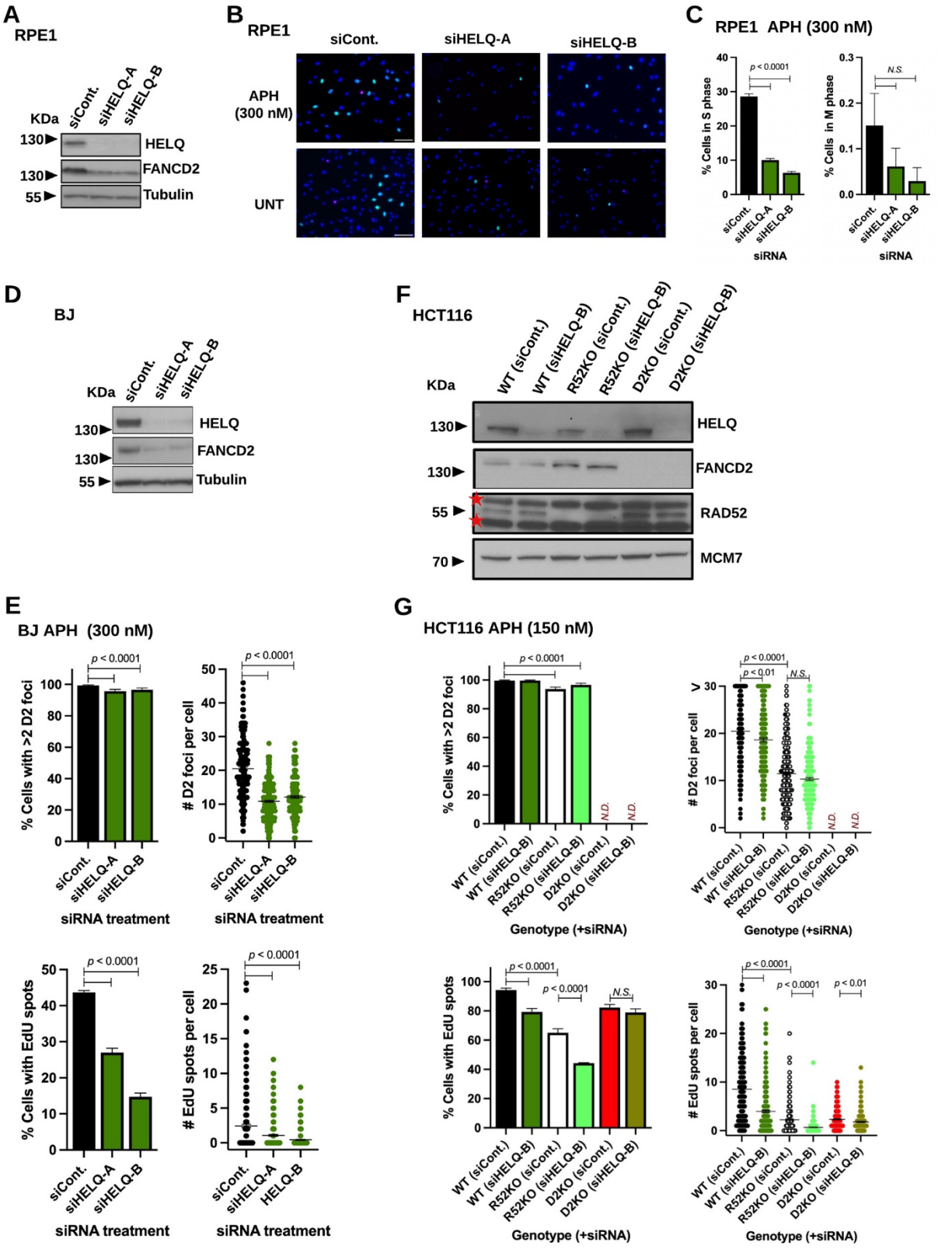

Supplemental Figure S6. HELQ depletion significantly decreases FANCD2 protein levels in RPE1 and BJ cells but not in HCT116 cells in which impaired MiDAS is observed only in the presence of FANCD2.

A) Immunoblotting of WCL confirming depletion of HELQ using two independent siRNAs in comparison to siControl treated conditions and unexpected co-depletion of FANCD2 in RPE1 cells. Tubulin was used as a loading control.

B) Representative microscope photos of RPE1 cells stained with EdU (green) and phospho-Histone H3 (red) showing a decrease in S phase cells upon siHELQ-A and -B treatment in comparison to siControl conditions. Nuclei were counterstained with DAPI (blue). Note that APH treatment accumulates S phase cells regardless of HELQ depletion (top) relative to untreated conditions (bottom). Scale bars indicate 100 μm.

C) Percentages of S phase cells (left) and those of M-phase cells (right) in HELQ-depleted and control conditions after APH treatment. Bars indicate standard errors. Significances were calculated using a χ^2 test.

D) Immunoblotting of WCL confirming depletion of HELQ in comparison to siControl treated conditions and consistent co-depletion of FANCD2 in BJ cells. Tubulin was used as a loading control.

E) Percentages of early M-phase cells with >2 FANCD2 (D2) foci (top left) or those with EdU spots (bottom left) as well as numbers of D2 foci (top right) and those of EdU spots per cell (bottom right) for BJ cells treated with siControl, siHELQ-A, or siHELQ-B. Bars indicate standard errors. Significances were calculated using a χ^2 test (left) or a Mann-Whitney test (right). Experiments were repeated at least three times, and a minimum of 300 nuclei were scored per treatment.

F) Immunoblotting of WCL confirming HELQ depletion in comparison to siControl treated conditions in WT, RAD52KO (R52KO) and D2KO HCT116 cells as well as the lack of RAD52 and FANCD2 in respective KO cells. MCM7 was used as a loading control. Red stars indicate nonspecific bands.

G) Percentages of early M-phase cells positive for >2 FANCD2 (D2) foci (top left) and those with EdU spots (bottom left) as well as numbers of D2 foci (top right) and those of EdU spots per cell (bottom right) for WT, R52KO, and D2KO HCT116 cells after treatment with siControl or siHELQ-B in APH-treated conditions.

In **E** and **G**, midlines indicate means on the right-side panels, and bars indicate standard errors. Experiments were repeated at least three times, and a minimum of 300 nuclei were scored per treatment. Pooled data (shown here) were analyzed for significances using a χ^2 test (left) or a Mann-Whitney test (right).

Supplemental Figure S7

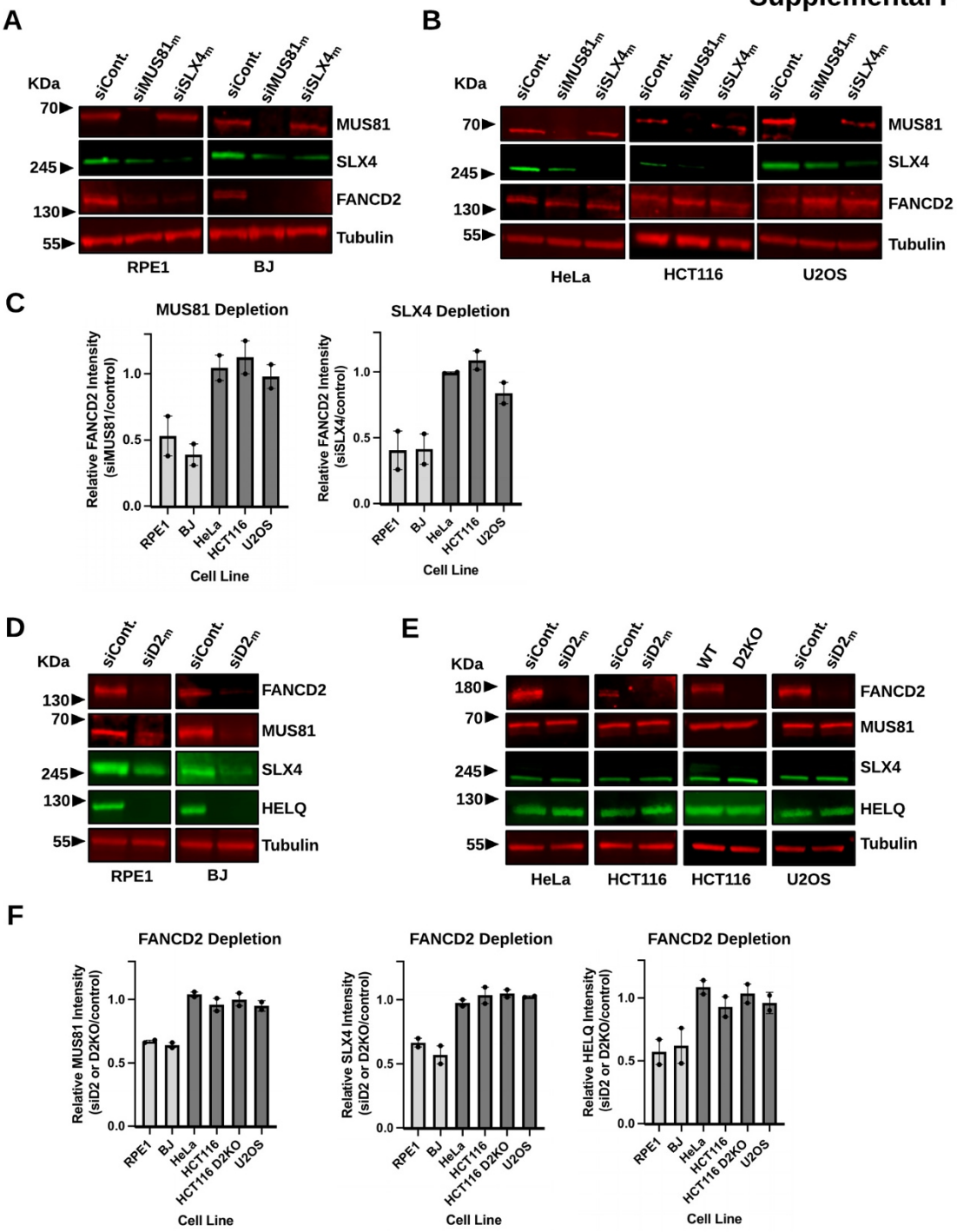

Supplemental Figure S7. Depletion of MUS81, SLX4, or HELQ reproducibly and reciprocally co-depletes FANCD2 in RPE1 and BJ cells but not HeLa, HCT116 or U2OS cells.
A) Representative fluorescent immunoblotting images showing *decreased* levels of FANCD2 in WCL made from RPE1 (left) and BJ (right) cells treated with ON-TARGETplus siMUS81$_m$ or siSLX4$_m$ compared to siControl-treated conditions.
B) Representative fluorescent immunoblotting images showing *unchanged* levels of FANCD2 in WCL made from HeLa (left), HCT116 (middle), and U2OS (right) cells treated with ON-TARGETplus siMUS81$_m$ or siSLX4$_m$ compared to siControl-treated conditions.
C) FANCD2 protein levels in RPE1, BJ, HeLa, HCT116, and U2OS cells after depletion of MUS81 (left) or SLX4 (right) relative to control conditions quantified from two independent experiments, one of which is shown in **A** and **B**. The column for each cell line indicates average relative FANCD2 intensity of two independent measurements (indicated by dots).
D) Representative fluorescent immunoblotting images showing *decreased* levels of MUS81, SLX4, and HELQ in WCL made from RPE1 (left) and BJ (right) cells treated with ON-TARGETplus siFANCD2$_m$ (siD2$_m$) compared to siControl-treated conditions.
E) Representative fluorescent immunoblotting images showing *unchanged* levels of MUS81, SLX4, and HELQ in WCL made from HeLa (far left), HCT116 (middle), and U2OS (far right) cells treated with ON-TARGETplus siD2$_m$ compared to siControl-treated conditions. In this analysis, we included the HCT116 D2KO clone which consistently display unchanged levels of MUS81, SLX4, and HELQ compared to HCT116 WT cells.
F) MUS81 (left), SLX4 (middle) and HELQ (right) protein levels in RPE1, BJ, HeLa, HCT116, and U2OS cells after depletion or knockout of FANCD2 relative to control conditions quantified from two independent experiments, one of which is shown in **D** and **E**. The column for each cell line indicates average relative intensity, with each independent experiment indicated by dots.
In **C** and **F** quantifications shown were normalized to the loading control and calculated relative to the siControl using Image Studio. Tubulin was used as a loading control.

References:

Bhowmick R, Minocherhomji S, Hickson ID. 2016. RAD52 Facilitates Mitotic DNA Synthesis Following Replication Stress. *Mol Cell* **64**: 1117-1126.

Boteva L, Nozawa RS, Naughton C, Samejima K, Earnshaw WC, Gilbert N. 2020. Common Fragile Sites Are Characterized by Faulty Condensin Loading after Replication Stress. *Cell Rep* **32**: 108177.

Minocherhomji S, Ying S, Bjerregaard VA, Bursomanno S, Aleliunaite A, Wu W, Mankouri HW, Shen H, Liu Y, Hickson ID. 2015. Replication stress activates DNA repair synthesis in mitosis. *Nature* **528**: 286-290.

Boteva L, Nozawa RS, Naughton C, Samejima K, Earnshaw WC, Gilbert N. 2020. Common Fragile Sites Are Characterized by Faulty Condensin Loading after Replication Stress. *Cell Rep* **32**: 108177.

Minocherhomji S, Ying S, Bjerregaard VA, Bursomanno S, Aleliunaite A, Wu W, Mankouri HW, Shen H, Liu Y, Hickson ID. 2015. Replication stress activates DNA repair synthesis in mitosis. *Nature* **528**: 286-290.

Mocanu C, Karanika E, Fernández-Casañas M, Herbert A, Olukoga T, Özgürses ME, Chan KL. 2022. DNA replication is highly resilient and persistent under the challenge of mild replication stress. *Cell Rep* **39**: 110701.

Supplemental Table S1:

Gene	Clone	Mutation sequence	Exon	sgRNA	Mutations
		RPE1			
FANCL	F1	Allele 1: CCTCCCCA(+AA)GTTCTACT Allele 2: CCTCC(+T)CCAGTTCTACT	Exon 5	antisense-stranded sgRNA 5' GAGTTCCTATCTCTTCAATA 3'	Biallelic frameshift
FANCL	F4	Allele 1: CCTCCT(-CC)CCAGTTCTACT Allele 2: CCTCCT(-C)CCCAGTTCTACT	Exon 5	antisense-stranded sgRNA 5' GAGTTCCTATCTCTTCAATA 3'	Biallelic frameshift
FANCI	C1	Allele 1: ACTTGTTGTATCC(+C)AGTT Allele 2: ACTTGTTG(-TATC)CAGTT	Exon 4	sense-stranded sgRNA 5' ATACACTTGTTGTATCCAGT 3	Biallelic frameshift
FANCI	C2	Allele 1: ACTTGTTGTATC(-C)AGTT Allele 2: ACTTGTTGTATCC(-A)GTT	Exon 4	sense-stranded sgRNA 5' ATACACTTGTTGTATCCAGT 3	Biallelic frameshift
FANCA	2A4	Allele 1: ttctc(-tccgtagCGGGAAGG)GTCAA Allele 2: ttctctccgtag(-CG)GGAAGGGTCAA	Intron 1/ Exon 2	sense-stranded sgRNA 5' gacttctctccgtagCGGGA 3'	Splice site Splice site or frameshift
FANCA	2A7	Allele 1: ttctctccgta(-gC)GGGAAGGGTCAA Allele 2:ttctctccgtagC(+GG)GGGAAGGGTCAA	Intron 1/ Exon 2	sense-stranded sgRNA 5' gacttctctccgtagCGGGA 3'	Splice site Splice site or frameshift
FANCE	C2	Allele 1: GACTGGGGTCGCTTG(+G)CTCG Allele 2: GACTGG(-GG)TCGCTTGCTCG	Exon 1	sense-stranded sgRNA 5' CGACTGGGGTCGCTTGCTCG 3'	Biallelic frameshift
FANCE	C6	Allele 1: GACTGGGGTCGCTTGCTC(+T)G Allele 2: GACTGGGGTC(-GC)TTGCTCGA	Exon 1	sense-stranded sgRNA 5' CGACTGGGGTCGCTTGCTCG 3'	Biallelic frameshift
		BJ			
FANCD2	13	Allele 1: GCCATGGATAC(-AC)TTG Allele 2: GCCATGGATACAC(+C)TTG	Exon 11	sense-stranded sgRNA 5' AACAGCCATGGATACACTTG 3'	Biallelic frameshift
FANCD2	10	Allele 1: GCCATGGATACAC(+A)TTG Allele 2: GCCATGGAT(-AC)ACTTG	Exon 11	sense-stranded sgRNA 5' AACAGCCATGGATACACTTG 3'	Biallelic frameshift

Supplemental Table S2:

Summary

Loci/Genotype	#Aberrations (Breaks) WT	D2KO (2B7)	D2KO (2C10)
Total	76(13)	108(10)	104(22)
CFS	**38(10)**	**59(6)**	**57(7)**
Non-CFS	38(3)	49(4)	47(15)

Regions affected	CFS	#Aberrations (Breaks) WT	D2KO (2B7)	D2KO (2C10)	All
Chromosome 1		8(1)	12	11(2)	31(1)
p22	FRA1D (p22)		3		3
p31-p32	FRA1C (p31.2)	4(1)	3	5(1)	12(2)
	FRA1L (p31)				
	FRA1B (p32)				
Q21	FRA1F (Q21)		2	1	3
Q31	FRA1K (Q31)			1	1
#CFS		**4(1)**	**8**	**7(1)**	**19**
#Non-CFS		4	4	4(1)	12(1)
Chromosome 2		7	12	13(4)	32(4)
p13	FRA2E (p13)			1	1
Q21-Q21.2	FRA2F (Q21.3)		3	4	7
Q31-Q33	FRA2G (Q31)	1	4		5
	FRA2H (Q32.1)				
	FRA2I (Q33)				
#CFS		**1**	**7**	**5**	**13**
#Non-CFS		6	5	8(4)	19(4)
Chromosome 3		8	12(2)	5(1)	25(1)
p14	FRA3B (p14.2)	3	1	1	5
Q25-Q27	FRA3D (Q25)	3	6	1	10
	FRA3C (Q27)				
	FRA3O (Q26.31)				
#CFS		**6**	**7**	**2**	**15**
#Non-CFS		2	5(2)	3(1)	10
Chromosome 4		9(2)	17(2)	17(3)	43(7)
p16	FRA4A (p16.1)			1	1
Q21-Q23	FRA4F (Q22.2)	1	4	6	11
Q31-Q34	Novel (Q32.2.)	5(2)	6(1)	3(1)	14(4)
	FRA4C (Q31.1)				
#CFS		**6(2)**	**10(1)**	**11(1)**	**27(4)**
#Non-CFS		3	7(1)	6(2)	16(3)
Chromosome 5		5(1)	10	4(1)	19(2)
p13-14	FRA5E (p14)		1	1	2
Q13.3-Q15	FRA5D (Q15)		1	2(1)	3(1)
Q22	FRA5F (Q21)	1	1	1	3
Q31	FRA5C (Q31.1)		2		2
#CFS		**1**	**5**	**4(1)**	**10(1)**
#Non-CFS		4(1)	5	0	9(1)
Chromosome 6		2	7(1)	9(2)	18(3)
Q21-Q21.3	FRA6F (Q21)		3	5	8
#CFS		**0**	**3**	**5**	**8**
#Non-CFS		2	4	4(2)	10(2)
Chromosome 7		14(6)	10(3)	10(3)	34(12)
p13	FRA7D (p13)	2			2
Q11.2-Q11.23	FRA7J (Q11)	6(5)	6(3)	3(1)	15(9)
Q22	FRA7F (Q22)	2	2	4(2)	8(2)
Q31-Q33	FRA7K (Q31.1)	3(1)	1	3	7(1)
	FRA7G (Q31.2)				
	FRA7H (Q32.3)				
#CFS		**13(6)**	**9(3)**	**10(3)**	**32(12)**
#Non-CFS		1	1	0	2

Regions affected	CFS	#Aberrations (Breaks) WT	D2KO (2B7)	D2KO (2C10)	All
Chromosome 8		3	4(1)	3	10(1)
Q21-Q22.3	FRA8B (Q22.1)		2(1)	2	4(1)
#CFS		**0**	**2(1)**	**2**	**4(1)**
#Non-CFS		3	2	1	6
Chromosome 9		3	2	5(1)	10(1)
Q22	FRA9D (Q22.1)			1(1)	1(1)
#CFS		**0**	**0**	**1(1)**	**1(1)**
#Non-CFS		3	2	4	9
Chromosome 10		3	6(1)	5	14(1)
Q22-Q22.1	FRA10D (Q22.2)	1	2	3	6
Q25	FRA10E (Q25.2)	1	1	1	3
Q26	FRA10F (Q26.1)		1		1
#CFS		**2**	**4**	**4**	**10**
#Non-CFS		1	2(1)	1	4(1)
Chromosome 11		2	2	2(1)	6(1)
Q13.5	FRA11H (Q13)	1			1
p15.1	FRA11C (p15.1)			1	1
#CFS		**1**	**0**	**1**	**2**
#Non-CFS		1	2	1(1)	4(1)
Chromosome 12		0	4	5(2)	9(2)
#CFS		**0**	**0**	**0**	**0**
#Non-CFS		0	4	5(2)	9(2)
Chromosome 13		2	2	2	6
Q21-Q21.2	FRA13C (Q21.2)		1	1	2
Q32	FRA13D (Q32)	1	1		2
#CFS		**1**	**2**	**1**	**4**
#Non-CFS		1	0	1	2
Chromosome 14		0	1(1)	1	2(1)
Q24.3	FRA14C (Q24.1)		1(1)		1(1)
#CFS		**0**	**1(1)**	**0**	**1(1)**
Non-CFS		0	0	1	1
Chromosome 15		1(1)	0	2(1)	3(2)
Q22	FRA15A (Q22)	1(1)			1(1)
#CFS		**1(1)**	**0**		**1(1)**
Non-CFS		0	0	2(1)	2(1)
Chromosome 16		3	3	2(1)	8(1)
Q22	FRA16C (Q22.1)	1		1	2
#CFS		**1**	**0**	**1**	**2**
#Non-CFS		2	3	1(1)	6(1)
Chromosome 17		1	1	1	3
#CFS		**0**	**0**	**0**	**0**
#Non-CFS		1	1	1	3
Chromosome 18		2(1)	1	3	6(1)
Q12.2	FRA18A (Q12.2)	1	1	1	3
Q21.1	FRA18B (Q21.3)			2	2
#CFS		**1**	**1**	**3**	**5**
#Non-CFS		1(1)	0	0	1(1)
Chromosome 19		No aberrations			
Chromosome 20		1(1)	1	0	2(1)
#CFS		**0**	**0**	**0**	**0**
#Non-CFS		1(1)	1	0	2(1)
Chromosome 21		1	0	1	2
#CFS		**0**	**0**	**0**	**0**
#Non-CFS		1	0	1	2(1)
Chromosome 22		No aberrations			
X Chromosome		1	1	3	5
#CFS		**0**	**0**	**0**	**0**
#Non-CFS		1	1	3	5

Note: Total numbers of aberrations for each chromosome are shown in bold orange with total numbers per genotype (clone) on the top summary table. These numbers are broken down to aberrations at CFS (shown in **bold**) and aberrations at Non-CFS in the summary table and individual chromosomes Loci highlighed in yellow are most frequently affected in our study.